Chemical Engineering Journal 164 (2010) 98–105

Contents lists available at ScienceDirect

Chemical Engineering Journal

journal homepage: www.elsevier.com/locate/cej

Fe-substituted nanometric $La_{0.9}K_{0.1}Co_{1-x}Fe_xO_{3-\delta}$ perovskite catalysts used for soot combustion, NO*x* storage and simultaneous catalytic removal of soot and NO*x*

Zhaoqiang Li[a], Ming Meng[a,*], Qian Li[a], Yaning Xie[b], Tiandou Hu[b], Jing Zhang[b]

[a] Tianjin Key Laboratory of Applied Catalysis Science and Engineering, School of Chemical Engineering & Technology, Tianjin University, Tianjin 300072, PR China
[b] Institute of High Energy Physics, Chinese Academy of Sciences, Beijing 100049, PR China

ARTICLE INFO

Article history:
Received 27 September 2009
Received in revised form 8 August 2010
Accepted 17 August 2010

Keywords:
Nanometric perovskite
Fe-substitution
NO*x* storage
Soot combustion
Simultaneous removal

ABSTRACT

A series of nanometric Fe-substituted $La_{0.9}K_{0.1}Co_{1-x}Fe_xO_{3-\delta}$ (x = 0, 0.05, 0.1, 0.2, 0.3) perovskite catalysts were prepared by citric acid complexation, which show novel activity for diesel soot oxidation, NO*x* storage, and simultaneous NO*x*–soot removal. Their structures and physical–chemical properties were examined by XRD, BET, SEM, XPS and EXAFS techniques. In $La_{0.9}K_{0.1}Co_{1-x}Fe_xO_{3-\delta}$ catalysts, the partial substitution of Co^{3+} by Fe^{3+} significantly enhances the catalytic activity towards soot oxidation or NO*x* storage and reduction. The catalyst $La_{0.9}K_{0.1}Co_{0.9}Fe_{0.1}O_{3-\delta}$ shows the highest activity for simultaneous NO*x*–soot removal, over which the maximal soot oxidation rate is achieved at only 362 °C (T_m), the NO*x* storage capacity reaches 213 μmol g^{-1}, and the percentage for NO*x* reduction by soot is 12.5%. Compared with the unsubstituted one ($La_{0.9}K_{0.1}CoO_{3-\delta}$), the activity enhancement of Fe-substituted samples results from the formation of high valence ion (Fe^{4+}) at B-site, relative high content of surface lattice oxygen and the high concentration of NO_2. Different from the widely accepted viewpoint that surface adsorbed oxygen species are responsible for soot combustion over perovskite catalysts, the surface lattice oxygen is identified as active oxygen species for soot combustion.

1. Introduction

Diesel engines have been widely employed in heavy- and light-duty vehicles because of their high fuel efficiency, low-operating cost and high durability. Compared with gasoline engines, they emit less CO and HC, however, the production of more NO*x* and particulate matters (soot) is unavoidable, which are extremely harmful to environment and human body. For example, the diesel particulates generally possess a size falling into the lung-damaging range (10–200 nm), and they contain many kinds of polycyclic aromatic hydrocarbons (PAH) and nitro-PAH in its soluble organic fraction (SOF), being potentially carcinogenic [1]. Recently, the emission regulations for diesel vehicles is becoming more and more strict, less than 5 mg km^{-1} for particulates and 80 mg km^{-1} for NO*x* will be prescribed by the pending 2014 Euro 6 regulations [2], so, it is urgent to control these two kinds of pollutants.

Up to now, plenty of research has been carried out worldwide on the removal of NO*x* and soot. For lean-burn nitrogen oxides, the NO*x* storage and reduction (NSR) catalysts are the most promising solution [3–5]. Over such kind of NSR catalysts the NO*x* conversion can reach 90% or higher [6]. For soot abatement, DPF (diesel particulates filter) technique is widely employed to trap the particulates, which are burned out by the oxidation catalysts deposited onto the filter [7,8]. In the last decade, simultaneous removal of NO*x* and soot has attracted much attention [9–13]. It is expected that both the NO*x* and soot can be removed in one single catalytic trap, which can lower not only the pressure drop but also the investment. However, highly efficient catalysts are still not found. So, the most urgent research topic is developing novel catalysts with high performance for simultaneous removal of NO*x* and soot at comparatively low temperatures possibly within the range typical of diesel exhaust: 200–400 °C [14].

Perovskite-type complex oxides possessing general formula ABO_3 often show higher chemical, thermal and structural stability than single oxides, as a result, exhibit better catalytic activity for many reactions. Several groups [15–17] reported that perovskite-type oxides are active for the simultaneous catalytic removal of NO*x* and soot. The most studied catalysts are the perovskites based on La at A-sites. The elements at B-sites are usually Co, Mn and Fe with changeable valence. Perovskite-type structure tolerates partial substitution of both A and B cations with other elements, which can result in the generation of oxygen vacancies or the change of chemical state for the elements at A- and/or B-site, as a result, the activity is often improved. Hong and Lee [17] reported that the activity

* Corresponding author. Tel.: +86 0 22 2789 2275; fax: +86 0 22 2789 2275.
E-mail address: mengm@tju.edu.cn (M. Meng).

1385-8947/$ – see front matter © 2010 Elsevier B.V. All rights reserved.
doi:10.1016/j.cej.2010.08.036

for soot oxidation in NO*x* atmosphere over La-based perovskites decreases in the following order: $LaCoO_3 > LaMnO_3 > LaFeO_3$; and the NO*x* reduction percentages over these catalysts follow almost the same sequence. In addition, the substitutional incorporation of K into A-sites of perovskites was found particularly effective on enhancing the activity and selectivity for the NO*x*–soot reaction [18–20]. However, for this reaction, the research focusing on simultaneous substitution of A- and B-site cations is seldom performed. It is reported that Fe-based perovskites possess good activity for soot combustion and NO*x* reduction [21,22], and the coordination radius of iron ion is larger than that for cobalt ion, so that the substitution of Co by Fe can promote the release of active oxygen in the reaction. In a word, the design of a NO*x*–soot removal catalyst based on $LaCoO_3$ perovskite with A and B sites partially substituted by K and Fe is feasible.

In the present work, Fe-substituted perovskite catalysts $La_{0.9}K_{0.1}CoO_3$, i.e., $La_{0.9}K_{0.1}Co_{1-x}Fe_xO_{3-\delta}$, were prepared by citric acid complexation [23], whose particle size is in nanometric scale. The effect of substitution amounts of Fe on the structures and catalytic performances of the catalysts for the simultaneous NO*x*–soot removal are investigated carefully. The essence of the activity enhancement arising from the Fe substitution, and the probable active oxygen species of the reaction are discussed.

2. Experimental

2.1. Catalyst preparation

A series of nanometric $La_{0.9}K_{0.1}Co_{1-x}Fe_xO_{3-\delta}$ ($x = 0, 0.05, 0.1, 0.2, 0.3$) perovskite catalysts were prepared by the citric acid complexation. $La(NO_3)_3{\cdot}6H_2O$, KNO_3, $Co(NO_3)_2{\cdot}6H_2O$ and $Fe(NO_3)_3{\cdot}6H_2O$ were used as precursors for obtaining an aqueous solution of La^{3+}, K^+, Co^{2+} and Fe^{3+} with the expected stoichiometry. A given amount of citric acid dissolved in deionized water was added in the above solution as a ligand, forming a homogeneous solution with a total concentration of 0.1 mol L^{-1} for all the cations. The molar amount of added citric acid is equal to that of all cations. The resulting solution was heated to the temperature of 80 °C under continuous stirring. The clear solution gradually turned into milky sol and finally transformed into gel, which was translucent with a honey-like color and viscosity. Then, the wet gel was dried homogenously in a stream of air at 120 °C overnight. Afterwards, the resulting loosened and foamy solid was heated to 200 °C in air by an electric furnace to remove the organic ligands. Successively, the precursor was heated to 400 °C and kept for 2 h to decompose the nitrates; at last, it was calcined at 700 °C for 4 h in static air. The final catalysts are denoted as LKCF*y*. Here, *y* stands for the substituting amount of Fe, e.g., $y = 5$ means that the substituting amount is 5%, namely $x = 0.05$ in $La_{0.9}K_{0.1}Co_{1-x}Fe_xO_{3-\delta}$. For comparison, the sample without Fe was also prepared at the same condition, which is denoted as LKC.

2.2. Catalyst characterization

X-ray diffraction measurement was carried out on an X' pert Pro rotatory diffractometer (PANAlytical Company) operating at 40 mA and 40 kV using Co Kα as radiation source ($\lambda = 0.1790$ nm). The data of 2θ from 20° to 100° were collected with a step size of 0.033.

The measurement of the specific surface area (SSA) was carried out at −196 °C on Quantachrome QuadraSorb SI instrument by using the nitrogen adsorption method. The samples were pretreated in vacuum at 300 °C for 8 h before experiments. The surface area (SSA) was determined by BET method in 0–0.3 partial pressure range.

The surface morphology was determined with a FEI NanoSEM 430 field emission-scanning electron microscope (FE-SEM) instrument.

X-ray photoelectron spectra (XPS) were recorded with a PHI-1600 ESCA spectrometer using Mg Kα radiation (1253.6 eV). The base pressure was 5×10^{-8} Pa. The binding energies were calibrated using C1s peak of contaminant carbon (B.E. = 284.6 eV) as standard, and quoted with a precision of ±0.2 eV. The surface composition of the samples in terms of atomic ratios was calculated, and Gaussian–Lorentzian and Shirley background was applied for peak analysis.

Extended X-ray absorption fine structure (EXAFS) measurements were carried out on the 1W1B beamline of Beijing Synchrotron Radiation Facility (BSRF) operating at about 120 mA and 2.5 GeV. The absorption spectra of the Co K-edge of samples and reference $LaCoO_3$ were recorded at room temperature in transmission mode. A Si (1 1 1) double-crystal monochromator was used to reduce the harmonic content of the monochrome beam. The back-subtracted EXAFS function was converted into *k* space and weighted by k^3 in order to compensate for the diminishing amplitude due to the decay of the photoelectron wave. The Fourier transforming of the k^3-weighted EXAFS data was performed in the range of $k = 3.4–14$ Å^{-1} with a Hanning function window.

2.3. Activity evaluation

For soot combustion, the catalytic activity of the prepared catalysts was evaluated by TG/DTA technique using Printex-U soot purchased from Degussa as the model reactant. The soot was mixed with the catalyst in a weight ratio of 1:20 in an agate mortar for 20 min to obtain a tight contact, which permits a high degree of reproducibility and sets a good basis for activity screening studies. The mixture was heated from 100 to 700 °C at a heating rate of 10 °C min^{-1} in the atmosphere of 600 ppm NO, 10 vol% O_2 and balance N_2 with a flow rate of 100 ml min^{-1}. By comparing characteristic temperatures of TG/DTA profiles, catalytic activity of samples was evaluated. In this work, soot ignition temperature (denoted as T_i), maximal combustion rate temperature of soot (denoted as T_m) and complete conversion temperature of soot (denoted as T_f) were used to evaluate the performance of the catalysts. Besides, TG/DTA experiments in the flow of air atmosphere were also carried out to compare the reactivity of soot combustion after exposing to NO-containing atmosphere or air.

For NO*x* removal, experiments were carried out in continuous fixed-bed quartz tubular reactor (i.d. = 8 mm) mounted in a tube furnace. The reaction temperature was controlled through a PID-regulation system based on the measurements of a K-type thermocouple and varied during each run from 100 to 700 °C at a heating rate of 10 °C min^{-1}. For the first run only the catalyst of 1.0 g was placed in the tubular quartz reactor, while for the second run the catalyst was replaced by the mixture of soot and catalyst (1:20, w/w). Reactant gases containing 600 ppm NO and 10 vol% O_2 balanced with N_2 passed through the catalyst bed at a flow rate of 400 ml min^{-1}. The gas hourly space velocity (GHSV) was about 40,000 h^{-1}. The outlet gases from the reactor were monitored by an on-line NO-NO_2-NO*x* Analyzer (Model 42i-HL, Thermo Scientific).

3. Results and discussion

3.1. XRD results

The XRD patterns of the $La_{0.9}K_{0.1}Co_{1-x}Fe_xO_{3-\delta}$ ($x = 0–0.3$) perovskite catalysts are shown in Fig. 1(a). All the main diffraction peaks of the Fe-substituted samples are in good agreement with the $LaCoO_3$ (JPCDS card: 48-0123), indicating that the samples maintain ABO_3 perovskite-type structure with rhombohedral space group after substitution. A very weak peak at $2\theta = 43°$ can be detected for all the samples, suggesting the presence of a small

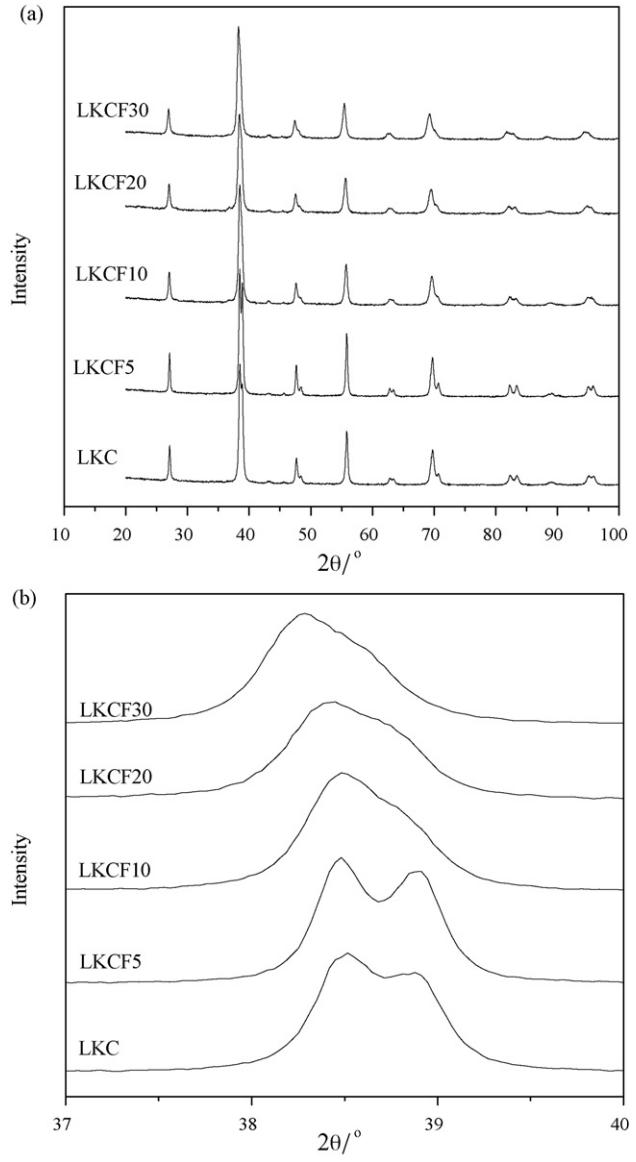

Fig. 1. XRD patterns of $La_{0.9}K_{0.1}Co_{1-x}Fe_xO_{3-\delta}$ catalysts: (a) full spectrum and (b) enlarged (1 1 0) reflections.

amount of Co_3O_4. With the Fe-substitution amount increasing, the intensity of the main diffraction peaks decreases gradually, which indicates that Fe-substitution decreases the crystallization degree. This is further confirmed by the EXAFS results in the following section. It should also be noted that the increase of Fe-substitution amount makes the main diffraction peaks shift to lower 2θ position gradually, as observed from the enlarged pattern in Fig. 1(b), evidencing that the relatively larger iron ion has been introduced into the perovskites structure.

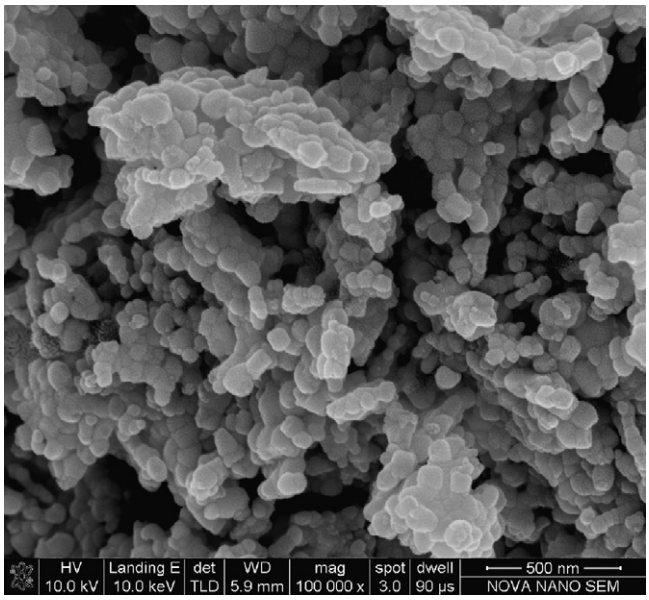

Fig. 2. FE-SEM photograph of $La_{0.9}K_{0.1}Co_{0.9}Fe_{0.1}O_{3-\delta}$ catalyst.

3.2. FE-SEM results

The morphology of $La_{0.9}K_{0.1}Co_{0.9}Fe_{0.1}O_{3-\delta}$ perovskite is presented in Fig. 2. It can be seen that most of the perovskite crystals range from 40 to 80 nm in size and exhibit a sphere-like shape. Since this size falls in the same order of magnitude as the diesel soot particulates (70–100 nm) [24], it is possible to achieve the highest specific number of contact points between the two counterparts. On the other hand, the relatively large size of soot particulates makes them hardly enter the pores of the perovskite catalysts. As a result, the outer surface of the catalysts is rather important during NO*x*–soot reaction, providing the necessary solid–solid contact sites [25]. In summary, the nanometric perovskite catalysts prepared by the citric acid complexation can provide the best contact conditions between catalyst and soot particulate, which is highly expected to promote the catalytic performance of the catalysts for the simultaneous NO*x*–soot removal.

3.3. XPS results

It is difficult to distinguish Co^{2+} and Co^{3+} from Co2p spectra due to the small difference in their binding energy, while the spin-orbit splitting of 2p peak (ΔE) is found to be well correlated with the Co oxidation state [26]. It is reported that the ΔE value of spin-orbit splitting for CoO is 16.0 eV [27] or 15.5 eV [28], and that of Co_2O_3 is 15.0 eV [29]. For Co_3O_4 with mixed valence of Co ions, a spin-orbit splitting value of 15.2 eV has been reported [30].

Fig. 3 and Table 1 show the XPS results of Co2p spectra for the $La_{0.9}K_{0.1}Co_{1-x}Fe_xO_{3-\delta}$ catalysts. According to Table 1, the ΔE value of Co2p in $La_{0.9}K_{0.1}CoO_3$ is 15.0 eV, which is mainly attributed to Co^{3+} since the K substitution amount is rather small, making most

Table 1
Co and O binding energy (B.E., eV) and the relative peak areas of lattice oxygen (O_{lat}) and adsorbed oxygen (O_{ads}) in $La_{0.9}K_{0.1}Co_{1-x}Fe_xO_{3-\delta}$ catalysts.

Catalyst	B.E. $Co2p_{3/2}$	B.E. $Co2p_{1/2}$	ΔE	O1s of O_{lat}		O1s of O_{ads}		O_{lat}/O_{ads}
				B.E.	Area ($\times 10^4$)	B.E.	Area ($\times 10^4$)	
LKC	780.6	795.6	15.0	529.3	4.27	531.8	7.48	0.57
LKCF5	779.6	794.9	15.3	528.6	4.81	531.1	7.64	0.63
LKCF10	779.6	795.2	15.6	528.6	5.25	531.1	6.64	0.79
LKCF20	779.6	794.9	15.3	528.7	4.44	531.3	6.56	0.68
LKCF30	779.6	794.9	15.3	528.6	4.61	531.0	6.68	0.69

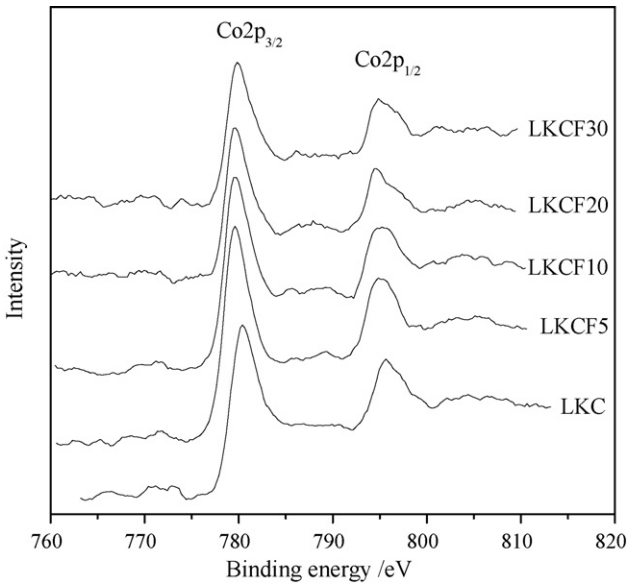

Fig. 3. XPS spectra for Co2p of $La_{0.9}K_{0.1}Co_{1-x}Fe_xO_{3-\delta}$ catalysts.

of the cobalt ions keep in the form of Co^{3+}. In the Fe-substituted samples of LKCF5, LKCF20 and LKCF30, the spin-orbit splitting value of Co2p is 15.3 eV, implying that the cobalt ions exist in the mixed valence states of +2 and +3. As a result, the average valence of cobalt ions in the perovskites is lower than +3. In order to maintain the electrical neutrality of perovskites, the positive charge reduced can be balanced either by the formation of higher oxidation state of the other B-site ions, i.e., part of Fe^{3+} ions transform into Fe^{4+}, or by the formation of oxygen vacancies. The ΔE value of 15.6 eV for Co2p in LKCF10 indicates that most of the cobalt ions are Co^{2+}, which suggests that more Fe^{4+} ions or more oxygen vacancies are formed in this sample, as compared with others.

The O1s XPS spectra of $La_{0.9}K_{0.1}Co_{1-x}Fe_xO_{3-\delta}$ catalysts are shown in Fig. 4. It is found that there are mainly two chemical states of oxygen in these samples. The peak with a low binding energy (~528.6 eV) is attributed to surface lattice oxygen, the other one with a high binding energy (~531.1 eV) is assigned to adsorbed oxygen species which may exist in oxygen vacancies of such defect oxides [31–33]. Due to the XPS peaks of O1s are not symmetric for these samples; they are fitted by a standard Gaussian–Lorentzian deconvolution method to get a relative content of different oxygen species corresponding to low and high binding energy. The deconvolution results are listed in Table 1. From Fig. 4 and Table 1, it can be seen that the binding energies of surface lattice oxygen of Fe-substituted samples are lower than that of the unsubstituted one, implying that the mobility of surface lattice oxygen is enhanced, thus the Fe-substituted samples potentially have higher activity for soot oxidation. For the ratio of lattice oxygen to adsorbed oxygen (O_{lat}/O_{ads}), it shows a volcano-like changing tendency with the increase of Fe-substitution amount. The O_{lat}/O_{ads} ratio of all the Fe-substituted samples is larger than that of the unsubstituted one (LKC). The catalyst LKCF10 possesses the largest O_{lat}/O_{ads} ratio of 0.79. The Shannon effective ionic radius of lanthanum and cobalt is 1.36 and 0.61 Å, respectively, whereas that for potassium and iron is 1.72 and 0.65 Å, respectively. Hence, the presence of relatively larger K and Fe in the perovskite lattice may enhance the release of active lattice oxygen species via the transformation of $Co^{3+} \rightarrow Co^{2+}$ and $Fe^{4+} \rightarrow Fe^{3+}$ during catalytic soot oxidation. As described above, the Fe-substituted samples possess relatively more surface lattice oxygen species, which show higher mobility, therefore, these substituted samples are expected to be more active towards soot oxidation than unsubstituted one.

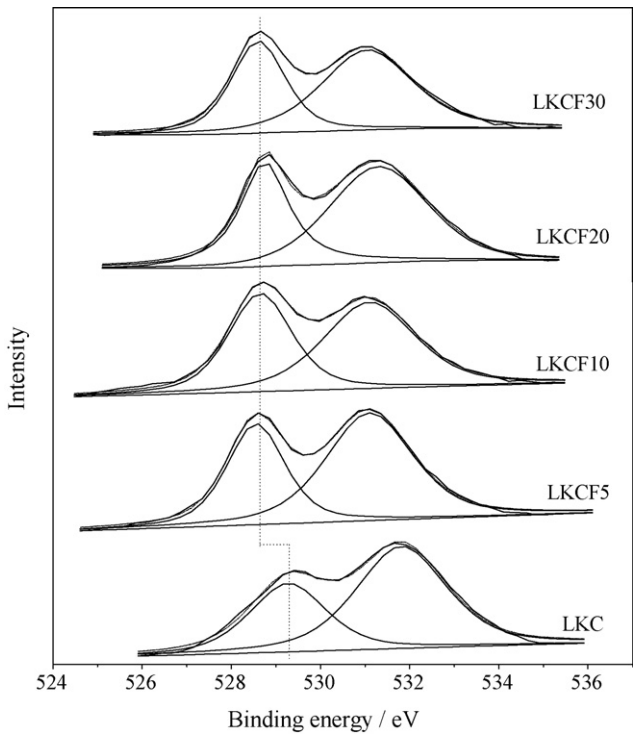

Fig. 4. XPS spectra for O1s of $La_{0.9}K_{0.1}Co_{1-x}Fe_xO_{3-\delta}$ catalysts.

3.4. EXAFS results

Fig. 5 shows the radial structural functions (RSFs) of Co K-edge for model $LaCoO_3$ and the prepared samples, derived from extended X-ray adsorption fine structure (EXAFS). The RSFs of the samples are well consistent with that of model $LaCoO_3$, evidencing that all the catalysts have formed the ABO_3 perovskite structure, which is manifested by the above XRD analysis. The RSFs show two major peaks corresponding to the first two coordination shells. The first peak at ~0.149 nm is assigned to octahedrally coordinated Co–O shell at 0.193 nm in $LaCoO_3$ perovskite, and the second one with maximum around 0.315 nm should contain contributions

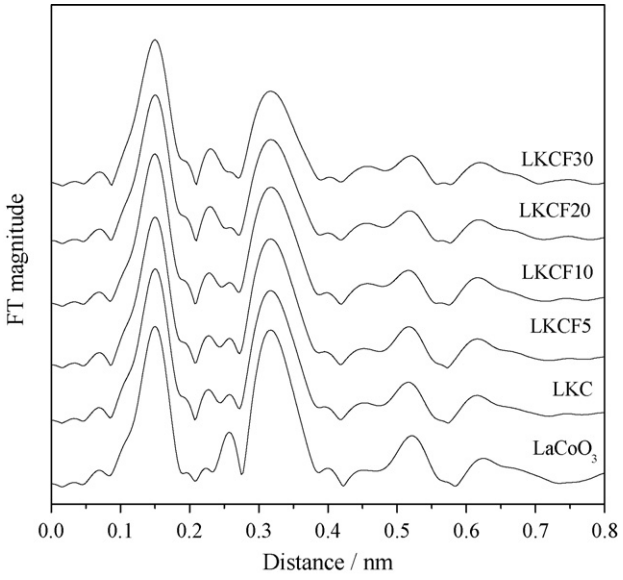

Fig. 5. Co K-edge RSFs of the catalysts and reference compounds.

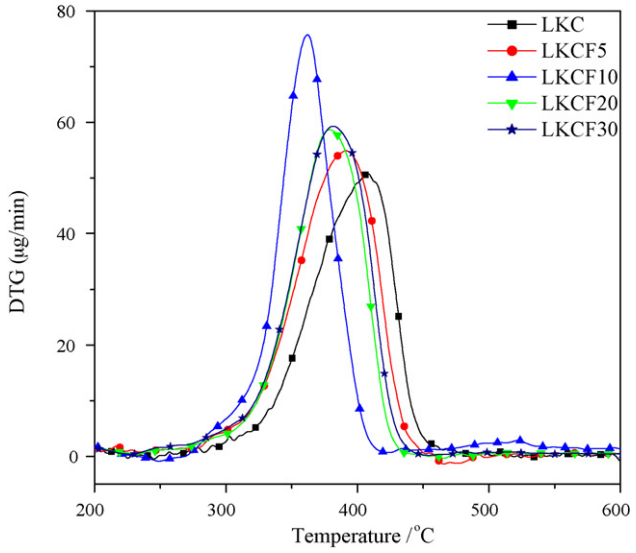

Fig. 6. DTG profiles of soot oxidation in the atmosphere of over 600 ppm NO + 10 vol% O_2 balanced by N_2 over $La_{0.9}K_{0.1}Co_{1-x}Fe_xO_{3-\delta}$ catalysts.

from single (Co–La, Co–Co) and multiple (Co–O–Co, Co–O–Co–O) scattering paths between 0.27 nm and 0.39 nm [34]. The intensity of the two major peaks, especially that for high coordination shells, decreases as the Fe-substitution amount increases. Generally, the peak corresponding to high coordination shells provides information of the crystallization degree of the corresponding metal or oxides [35,36]. So, it is deduced that the crystallite size of the prepared perovskites gradually decreases with the Fe substitution amount increasing. This is in good agreement with the previous XRD results.

3.5. Catalytic performance

3.5.1. Catalytic activity for soot combustion

The soot combustion experiment was carried out on a TG/DTA setup in the atmosphere of 600 ppm NO, 10 vol% O_2 and balance N_2 with the temperature range of 100–700 °C. The results are shown in Fig. 6 and listed in Table 2. The characteristic temperature of T_i, T_m, T_f and ΔT ($T_f - T_i$) are used to denote the activity of the catalysts for soot oxidation. It can be seen that the T_m of the sample LKC is about 409 °C, which is remarkably lowered after Fe-substitution. The soot oxidation activity shows a typical volcano tendency with the Fe-substitution amount increasing. The activity decreases in following sequence: LKCF10 > LKCF20 ≈ LKCF30 > LKCF5 > LKC. The T_m of the most active LKCF10 sample is only 362 °C, which is the lowest value among all the samples, about 47 °C lower than that for LKC. Moreover, the ΔT of the LKCF10 (178 °C) is also the lowest, indicating that the average soot combustion rate on LKCF10 is higher than those on other samples.

Since the diesel soot particulates can easily accumulate on the particulate filter, it is necessary to regenerate the filter periodically in air. Hence, in this work, the soot oxidation behavior in air is also studied. The DTG profiles are shown in Fig. S1. It can be seen that the activity order for soot oxidation in air is identical with that in the atmosphere containing NO above. The LKCF10 sample still shows the highest activity, with the T_m at 380 °C and ΔT equal to 191 °C, respectively.

According to XRD and EXAFS results, the major phases of the prepared samples are perovskite-type oxides with the presence of a very small amount of Co_3O_4. Wang et al. [37] reported that the activity of Co_3O_4 for soot oxidation is lower than that of $La_{0.9}K_{0.1}CoO_3$ perovskite. So, it is deduced that the perovskite oxides are responsible for the high activity of the samples for soot combustion.

The soot removal reaction supposedly takes place at triple phase boundary of a solid catalyst, a solid reactant and gaseous reactants (NO, O_2). Hence, the contact conditions between soot and the catalytic active sites are significantly important for this kind of solid–solid reactions [38–40]. Liu et al. [41] even thought that the contact conditions between catalysts and soot is a rate-determining factor because the number of contact points on the catalysts is proportional to the active site concentration. In the present work, the particle size of the prepared nanometric $La_{0.9}K_{0.1}Co_{1-x}Fe_xO_{3-\delta}$ catalysts is about 40–80 nm, which falls in the same order of magnitude as that of soot, ensuring high contacting efficiency between the two counterparts. Furthermore, when the B-site cations of $La_{0.9}K_{0.1}CoO_3$ are partly substituted by Fe^{3+}, some iron ions (Fe^{4+}) with higher oxidation state are formed according to the Co2p XPS spectra. The tetravalent iron ion possesses higher catalytic oxidation activity than Fe^{3+} and Co^{3+}, lowering the soot oxidation temperature. Fig. 3 and Table 1 show that some iron ions in all the Fe-substituted samples have transformed to tetravalent iron ions, and the sample LKCF10 possesses the largest amount of Fe^{4+}. This is consistent with its highest catalytic activity for soot combustion. On the other hand, when Co^{3+} ions are partly replaced by Fe^{3+} ions, some oxygen vacancies may be generated in order to maintain the electron neutrality. The presence of large amount of oxygen vacancies would enhance the mobility of lattice oxygen and accelerate the transferring of oxygen species, meanwhile, oxygen vacancies also facilitate the adsorption and activation of NO, improving the catalytic activity for simultaneous removal of soot and NO*x*, as elucidated in the next section.

It is generally thought that perovskites can desorb two different types of oxygen species, namely adsorbed oxygen and lattice oxygen [42–45]. The surface adsorbed oxygen, weakly chemisorbed on the perovskite, strongly depends on the surface oxygen vacancies. Its nature depends on the degree of the substitution of A-site ions by other lower valence ions, and also on the character of B-site ions in ABO_3 structure [43]. On the contrary, the desorption of lattice oxygen, only related to the nature of B-site ions, is linking to the redox transitions of the valence state of B-site ions, which are Co and Fe in this study. Fino et al. [46,47] thought that the surface adsorbed oxygen (O^-) of perovskite catalysts participates in soot combustion reaction, determining the activity of the catalysts for the soot oxidation. Liu et al. [29,41] found three different kinds of oxygen species in perovskite-like complex oxide catalysts, namely O_2^-, O^- and O^{2-}, and it is thought that the O_2^- and O^- species are responsible for soot oxidation.

Table 2
Specific surface areas (SSA), temperatures of soot combustion, NO*x* storage capacities (NSC) and NO*x* reduction percentages of $La_{0.9}K_{0.1}Co_{1-x}Fe_xO_{3-\delta}$ catalysts.

Catalysts	SSA ($m^2\ g^{-1}$)	T_i (°C)	T_m (°C)	T_f (°C)	ΔT (°C)	NSC ($\mu mol\ g^{-1}$)	NO*x* reduction percentage (%)
LKC	3.8	252	409	526	274	90 (100–346 °C)	11.9 (323–368 °C)
LKCF5	6.6	276	392	474	198	129 (100–342 °C)	6.2 (290–700 °C)
LKCF10	9.4	251	362	429	178	213 (100–394 °C)	12.5 (306–700 °C)
LKCF20	6.0	251	379	463	214	115 (100–348 °C)	4.5 (272–498 °C)
LKCF30	6.6	255	382	450	195	110 (100–374 °C)	0.7 (277–466 °C)

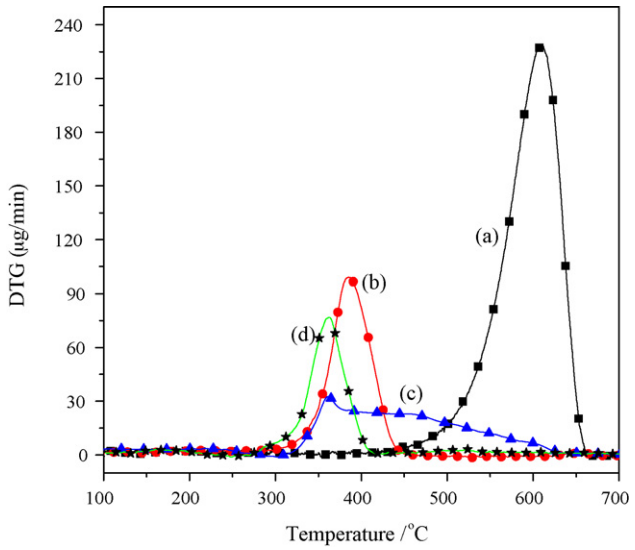

Fig. 7. DTG profiles of soot combustion at different reaction conditions. (a) 600 ppm NO + 10 vol% O_2 + balance N_2 without catalyst; (b) 10 vol% O_2 + balance N_2 with catalyst $La_{0.9}K_{0.1}Co_{0.9}Fe_{0.1}O_{3-\delta}$; (c) 600 ppm NO + balance N_2 with catalyst $La_{0.9}K_{0.1}Co_{0.9}Fe_{0.1}O_{3-\delta}$; (d) 600 ppm NO + O_2 + balance N_2 with catalyst $La_{0.9}K_{0.1}Co_{0.9}Fe_{0.1}O_{3-\delta}$.

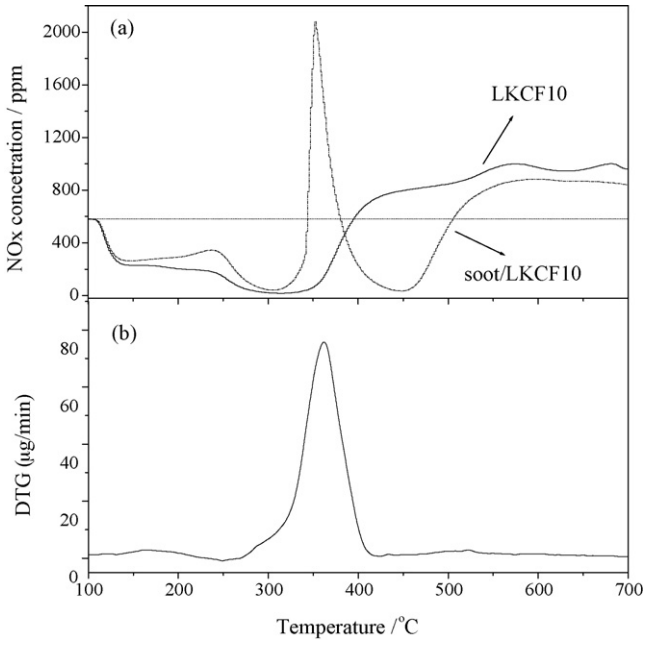

Fig. 8. (a) Outlet NO*x* concentration over $La_{0.9}K_{0.1}Co_{0.9}Fe_{0.1}O_{3-\delta}$ and soot/$La_{0.9}K_{0.1}Co_{0.9}Fe_{0.1}O_{3-\delta}$ and (b) soot combustion over $La_{0.9}K_{0.1}Co_{0.9}Fe_{0.1}O_{3-\delta}$. Reaction conditions: NO = 600 ppm, O_2 = 10 vol% balanced by N_2.

However, in this study the situation may be different. According to the results of O1s XPS spectra (Fig. 4 and Table 1), the relative content of surface lattice oxygen decreases as follows: LKCF10 > LKCF20 ≈ LKCF30 > LKCF5 > LKC, which is consistent with the activity order for soot combustion, implying that the surface lattice oxygen species in perovskite catalysts is mainly account for the soot combustion behavior. Moreover, the binding energy of surface lattice oxygen is lowered when the B-site cation (Co^{3+}) is substituted by Fe, increasing the mobility of surface lattice oxygen towards soot oxidation. The relative larger K^+ and Fe^{3+} in the perovskite lattice may enhance the release of active lattice oxygen species associated to $Co^{3+} \rightarrow Co^{2+}$ and $Fe^{4+} \rightarrow Fe^{3+}$ transitions, in addition, the presence of large amount of oxygen vacancies also facilitates the capture of gaseous oxygen and enhances the mobility of surface lattice oxygen. Thus, the Fe-substituted samples show higher activity for soot oxidation than the unsubstituted one.

Fig. 7 shows the DTG profiles of soot oxidation on LKCF10 catalyst at various reaction conditions. In the absence of catalyst, as displayed in Fig. 7(a), soot oxidation takes place at rather high temperature (above 400 °C) in the atmosphere of 10 vol% O_2, 600 ppm NO and balance N_2, with the T_m at approximately 578 °C. However, the typical temperature of diesel exhaust is between 200 and 400 °C, non-catalysis process is hard to remove the soot particulates. In the presence of catalyst LKCF10, soot oxidation in the atmosphere of 10 vol% O_2 and balance N_2 without NO is remarkably accelerated with the T_m at about 386 °C, as shown in Fig. 7(b). The DTG profiles of soot oxidation in the absence of oxygen are presented in Fig. 7(c). It is thought that soot is oxidized by surface lattice oxygen in this situation, and the T_i and T_f, especially the T_f, is rather high, which are 310 °C and 700 °C, respectively. In the presence of NO and oxygen, as shown in Fig. 7(d), the temperature of soot maximal combustion rate is decreased to 362 °C. Comparing Fig. 7(d) and Fig. 7(a), it is found that the presence of LKCF10 catalyst can lower the T_m more than 200 °C. Additionally, by comparing Fig. 7(d) with Fig. 7(b) and (c), it is found that the T_m is lower and the soot combustion rate is much higher in the presence of both NO and O_2. Fig. S2 presents the profiles of the effluent NO_2 concentration over different samples. From this figure, it can be seen that the NO_2 concentration of all the Fe-substituted samples is higher than that of unsubstituted one, and the NO_2 concentration of LKCF10 sample is the largest among all the samples. Therefore, it is inferred that NO is oxidized to NO_2 by oxygen in the presence of catalyst, and the formed NO_2 exhibits higher activity for soot oxidation than NO and oxygen, similar conclusion is also drawn in references [48,49].

3.5.2. NO*x* storage and simultaneous soot–NO*x* removal over $La_{0.9}K_{0.1}Co_{1-x}Fe_xO_{3-\delta}$

The profiles of NO*x* storage capacity (NSC) on $La_{0.9}K_{0.1}Co_{1-x}Fe_xO_{3-\delta}$ are presented in Fig. S3. The dash line in the figure represents the NO*x* concentration in the gas feed, and the points below and above the line mean the occurrence of NO*x* sorption and NO*x* desorption, respectively [50]. The NSC values are calculated according to peak areas of NO*x* uptake curves, which are listed in Table 2. It can be found that the NO*x* uptake temperature ranges from 100 to 390 °C. In addition, all the Fe-substituted samples exhibit larger amounts of NSC than the unsubstituted one, the sample LKCF10 shows the maximal NO*x* uptake amount of 213 μmol g^{-1} among all the samples, and the other Fe-substituted samples possess similar NO*x* uptake amounts. The results are well correlated with the specific surface areas (SSA) of these samples; larger surface area corresponds to higher NSC. On the other hand, the Fe-substituted samples possess higher oxidation activity, which is related to the formation of more NO_2 (as described above), so it is suggested that NO can be more efficiently oxidized to NO_2 over the Fe-substituted samples. The formed NO_2 can be stored more easily on the catalyst than NO.

Fig. 8(a) displays the profiles of effluent gas from LKCF10 and soot/LKCF10 mixtures during the heating process (10 °C min^{-1}) in a gas feed of 600 ppm NO, 10 vol% O_2 and balance N_2. The dash line in the figure represents the NO*x* concentration in the stream, and the points below and above the line mean the occurrence of NO*x* sorption/reduction and NO*x* desorption, respectively. The LKCF10 sample presents NO*x* uptake between 100 and 394 °C, followed by a broad NO*x* desorption at higher temperature. Due to the temperature limitation of the fixed-bed reactor, NO*x* desorption is not completely finished at 700 °C, so, the desorption profile did not come back to the original baseline, and the amount of NO*x* desorption should be a little lower than that of NO*x* adsorp-

tion. According to the observed areas below and above the dotted line, the calculated results of NO*x* sorption amount (213 μmol g^{-1}) and desorption amount (192 μmol g^{-1}) are close to each other. For soot/LKCF10 mixture there are two adsorption/reduction regions and two desorption regions. At low temperatures (≤340 °C), NO*x* uptake is similar to that of LKCF10, but the situation is noticeably different at higher temperature. Unlike the case of LKCF10 alone, a very sharp NO*x* desorption peak appears at 344 °C, just after the onset of the soot combustion, as seen in Fig. 8(b). Clearly, the sharp desorption of NO*x* is initiated by the very fast and local exotherm from soot combustion. After this, NO*x* concentration suddenly drops below the dotted line, evidencing the occurrence of NO*x* reduced by soot. Moreover, the observed area below the dotted line is much larger than that above it, corresponding to 235 μmol of NO*x* g^{-1} and 142 μmol of NO*x* g^{-1}, respectively, which suggests that partial NO*x* must have reacted with soot during the heating process.

In order to compare the catalytic performance for simultaneous removal of NO*x* and soot over different catalysts, the NO*x* reduction level is evaluated by comparing the NO*x* sorption and desorption over the catalysts mixed with soot or not, the results of which are listed in Table 2. It can be seen that the LKCF10 sample possesses the largest NO*x* reduction percentage of 12.5%. Combined with the results for soot combustion and NO*x* storage, the Fe-substituted perovskite catalyst LKCF10 is the most promising candidate for practical purification of diesel emission.

4. Conclusions

The partial substitution of Co^{3+} by Fe^{3+} in $La_{0.9}K_{0.1}Co_{1-x}Fe_xO_{3-\delta}$ (x = 0–0.3) perovskite catalysts largely improves the catalytic activity of the catalyst $La_{0.9}K_{0.1}CoO_{3-\delta}$ for soot combustion, NO*x* storage and simultaneous soot–NO*x* removal. Among all the prepared catalysts the $La_{0.9}K_{0.1}Co_{0.9}Fe_{0.1}O_{3-\delta}$ perovskite is the most active one, over which the temperature corresponding to maximal rate of soot combustion (T_m) is only 362 °C, and the temperature region for soot oxidation is narrowed in 178 °C. For NO*x* storage and reduction, $La_{0.9}K_{0.1}Co_{0.9}Fe_{0.1}O_{3-\delta}$ perovskite also shows a high NO*x* storage capacity of 213 μmol g^{-1} and a satisfied NO*x* reduction percentage of 12.5%.

The high catalytic activity of Fe-substituted $La_{0.9}K_{0.1}Co_{1-x}Fe_xO_{3-\delta}$ perovskite catalysts can be elucidated from following aspects: firstly, the size of the obtained nanometric catalysts falls in the same order of magnitude as that for diesel soot particulates, ensuring a high contacting efficiency between soot particles and catalysts; secondly, the Fe-substituted $La_{0.9}K_{0.1}Co_{1-x}Fe_xO_{3-\delta}$ perovskite catalysts, especially $La_{0.9}K_{0.1}Co_{0.9}Fe_{0.1}O_{3-\delta}$, possess higher content of surface lattice oxygen, which can be well correlated with the soot oxidation activity of the catalysts, meanwhile, the Fe-substitution enhances the mobility of surface lattice oxygen, further improving their catalytic activity for soot combustion; thirdly, the formation of high valence ion (Fe^{4+}) at B-site increases the oxidation ability of the catalysts, especially $La_{0.9}K_{0.1}Co_{0.9}Fe_{0.1}O_{3-\delta}$, which facilitates the oxidation of NO to NO_2, accelerating the NO*x* storage and the simultaneous soot–NO*x* reaction.

Acknowledgements

This work is financially supported by the National Natural Science Foundation of China (Nos. 20876110 and 21076146), the Specialized Research Fund for the Doctoral Program of Higher Education of China (No. 20090032110013), the Program of New Century Excellent Talents in University of China (No. NCET-07-0599) and the "863" Programs of the Ministry of Science and Technology of China (No. 2008AA06Z323). The authors are also grateful to the Cheung Kong Scholar Program for Innovative Teams of the Ministry of Education (No. IRT0641) and the Program of Introducing Talents of Discipline to University of China (No. B06006).

Appendix A. Supplementary data

Supplementary data associated with this article can be found, in the online version, at doi:10.1016/j.cej.2010.08.036.

References

[1] D. Fino, Diesel emission control: catalytic filters for particulate removal, Sci. Technol. Adv. Mater. 8 (2007) 93–100.
[2] T.V. Johnson, Diesel Emission Control in Review, SAE Paper No. 2007-01-0233, 2007.
[3] S. Matsumoto, Catalytic reduction of nitrogen oxides in automotive exhaust containing excess oxygen by NO*x* storage-reduction catalyst, Cattech 4 (2000) 102–109.
[4] Y. Liu, M. Meng, X.G. Li, L.H. Guo, Y.Q. Zha, NO*x* storage behavior and sulfur-resisting performance of the third-generation NSR catalysts Pt/K/TiO_2–ZrO_2, Chem. Eng. Res. Des. 86 (2008) 932–940.
[5] Y. Liu, M. Meng, Z.Q. Zou, X.G. Li, Y.Q. Zha, In situ DRIFTS investigation on the NO*x* storage mechanisms over Pt/K/TiO_2–ZrO_2 catalyst, Catal. Commun. 10 (2008) 173–177.
[6] W.S. Epling, L.E. Campbell, A. Yezerets, N.W. Currier, J.E. Parks, Overview of the fundamental reactions and degradation mechanisms of NO*x* storage/reduction catalysts, Catal. Rev. 46 (2004) 163–245.
[7] B.A.A.L. van Setten, M. Makkee, J.A. Moulijn, Science and technology of catalytic diesel particulate filters, Catal. Rev. 43 (2001) 489–564.
[8] M.M. Maricq, Chemical characterization of particulate emissions from diesel engines: a review, Aero. Sci. 38 (2007) 1079–1118.
[9] K. Yoshida, S. Makino, S. Sumiya, G. Muramatsu, R. Helferich, Simultaneous Reduction of NOx and Particulate Emissions from Diesel Engine Exhaust, SAE Paper No. 892046, 1989.
[10] N. Nejar, M.J. Illan-Gomez, Potassium–copper and potassium–cobalt catalysts supported on alumina for simultaneous NO*x* and soot removal from simulated diesel engine exhaust, Appl. Catal. B: Environ. 70 (2007) 261–268.
[11] N. Russo, S. Furfori, D. Fino, G. Saracco, V. Specchia, Lanthanum cobaltite catalysts for diesel soot combustion, Appl. Catal. B: Environ. 83 (2008) 85–95.
[12] Q. Li, M. Meng, Z.Q. Zou, X.G. Li, Y.Q. Zha, Simultaneous soot combustion and nitrogen oxides storage on potassium-promoted hydrotalcite-based CoMgAlO catalysts, J. Hazard. Mater. 161 (2009) 366–372.
[13] Q. Li, M. Meng, N. Tsubaki, X.G. Li, Z.Q. Li, Y.N. Xie, T.D. Hu, J. Zhang, Performance of K-promoted hydrotalcite-derived CoMgAlO catalysts used for soot combustion, NO*x* storage and simultaneous soot–NO*x* removal, Appl. Catal. B: Environ. 91 (2009) 406–415.
[14] L. Sui, L.Y. Yu, Diesel soot oxidation catalyzed by Co–Ba–K catalysts: evaluation of the performance of the catalysts, Chem. Eng. J. 142 (2008) 327–330.
[15] Y. Teraoka, K. Nakano, S. Kagawa, W.F. Shangguan, Simultaneous removal of nitrogen oxides and diesel soot particulates catalyzed by perovskite-type oxides, Appl. Catal. B: Environ. 5 (1995) L181–185.
[16] Y. Teraoka, K. Nakano, W.F. Shangguan, S. Kagawa, Simultaneous catalytic removal of nitrogen oxides and diesel soot particulate over perovskite-related oxides, Catal. Today 27 (1996) 107–113.
[17] S.S. Hong, G.D. Lee, Simultaneous removal of NO and carbon particulates over lanthanoid perovskite-type catalysts, Catal. Today 63 (2000) 239–404.
[18] W.F. Shangguan, Y. Teraoka, S. Kagawa, Promotion effect of potassium on the catalytic property of $CuFe_2O_4$ for the simultaneous removal of NO*x* and diesel soot particulate, Appl. Catal. B: Environ. 16 (1998) 149–154.
[19] Y. Teraoka, K. Nakano, S. Kagawa, Synthesis of La–K–Mn–O perovskite-type oxides and their catalytic property for simultaneous removal of NO*x* and diesel soot particulates, Appl. Catal. B: Environ. 34 (2001) 73–78.
[20] T. Miyazaki, N. Tokabuchi, M. Arita, M. Inoue, I. Mochida, Catalytic combustion of carbon by alkali metal carbonates supported on perovskite-type oxide, Energy Fuel 11 (1997) 832–836.
[21] K. Taniguchi, T. Hirano, T. Tosho, T. Akiyama, Mechanical activation of self-propagating high-temperature synthesized $LaFeO_3$ to be used as catalyst for diesel soot oxidation, Catal. Lett. 130 (2009) 362–366.
[22] S. Furfori, S. Bensaid, N. Russo, D. Fino, Towards practical application of lanthanum ferrite catalysts for NO reduction with H_2, Chem. Eng. J. 154 (2009) 348–354.
[23] M.M. Natile, E. Ugel, C. Maccato, A. Glisenti, $LaCoO_3$: effect of synthesis conditions on properties and reactivity, Appl. Catal. B: Environ. 72 (2007) 351–362.
[24] M. Kostoglou, P. Housiada, A.G. Konstandopoulos, Multi-channel simulation of regeneration in honeycomb monolithic diesel particulate filters, Chem. Eng. Sci. 58 (2003) 3273–3283.
[25] J. Liu, Z. Zhao, C.M. Xu, A.J. Duan, Simultaneous removal of NO*x* and diesel soot over nanometer Ln–Na–Cu–O perovskite-like complex oxide catalysts, Appl. Catal. B: Environ. 78 (2008) 61–72.
[26] J.Y. Luo, M. Meng, X. Li, X.G. Li, Y.Q. Zha, T.D. Hu, Y.N. Xie, J. Zhang, Mesoporous Co_3O_4–CeO_2 and Pd/Co_3O_4–CeO_2 catalysts: synthesis, characterization

and mechanistic study of their catalytic properties for low-temperature CO oxidation, J. Catal. 254 (2008) 310–324.
[27] K. Ichimura, Y. Inoue, I. Yasumori, Catalysis by mixed oxide perovskites. I. Hydrogenolysis of ethylene and ethane on $LaCoO_3$, Bull. Chem. Soc. Jpn. 53 (1980) 3044–3049.
[28] D.C. Frost, C.A. Mcdowell, I.S. Woolsey, X-ray photoelectron spectra of cobalt compounds, Mol. Phys. 27 (1974) 1473–1489.
[29] Z.M. Liu, J.M. Hao, L.X. Fu, T.L. Zhu, Study of Ag/La0.6Ce0.4CoO_3 catalysts for direct decomposition and reduction of nitrogen oxides with propene in the presence of oxygen, Appl. Catal. B: Environ. 44 (2003) 355–370.
[30] D.V. Cesar, C.A. Peréz, M. Schmal, V.M.M. Salim, Quantitative, XPS analysis of silica-supported Cu–Co oxides, Appl. Surf. Sci. 157 (2000) 159–166.
[31] R.Q. Tan, Y.F. Zhu, Poisoning mechanism of perovskite $LaCoO_3$ catalyst by organophosphorous gas, Appl. Catal. B: Environ. 58 (2005) 61–68.
[32] Z. Zhao, X. Yang, Y. Wu, Comparative study of nickel-based perovskite-like mixed oxide catalysts for direct decomposition of NO, Appl. Catal. B: Environ. 8 (1996) 281–297.
[33] Y. Wu, T. Wu, B.S. Dou, C.X. Wang, X.F. Xie, Z.L. Yu, S.R. Fan, Z.R. Fan, L.C. Wang, A comparative study on perovskite-type mixed oxide catalysts $A'_xA_{1-x}BO_{3-\lambda}$ (A' = Ca, Sr, A = La, B = Mn, Fe, Co) for NH_3 oxidation, J. Catal. 120 (1989) 88–107.
[34] O. Haas, R.P.W.J. Struis, J.M. McBreen, Synchrotron X-ray absorption of $LaCoO_3$ perovskite, J. Solid State Chem. 177 (2004) 1000–1010.
[35] O.V. Komova, A.V. Simakov, V.A. Rogov, D.I. Kochubei, G.A. Odegova, V.V. Kriventsov, E.A. Paukshtis, V.A. Ushakov, N.N. Sazonova, T.A. Nikoro, Investigation of the state of copper in supported copper–titanium oxide catalysts, J. Mol. Catal. A: Chem. 161 (2000) 191–204.
[36] J.R. Chang, S.L. Chang, T.B. Lin, γ-Alumina supported Pt catalysts for aromatics reduction: a structural investigation of sulfur poisoning catalyst deactivation, J. Catal. 169 (1997) 338–346.
[37] H. Wang, P. Liang, C.M. Xu, A.J. Duan, G.Y. Jiang, J. Xu, J. Liu, Highly active $La_{1-x}K_xCoO_3$ perovskite-type complex oxide catalysts for the simultaneous removal of diesel soot and nitrogen oxides under loose contact conditions, Catal. Lett. 124 (2008) 91–99.
[38] J.V. Craenenbroeck, D. Andreeva, T. Tabakova, K.V. Werde, J. Mullens, F. Verpoort, Spectroscopic analysis of Au–V-based catalysts and their activity in the catalytic removal of diesel soot particulates, J. Catal. 209 (2002) 515–527.
[39] P.A.J. Neeft, M. Makkee, J.A. Moulijn, Catalysts for the oxidation of soot from diesel exhaust gases: I. An exploratory study, Appl. Catal. B: Environ. 8 (1996) 57–78.
[40] A. Carrascull, I.D. Lick, N.P. Esther, M.I. Ponzi, Catalytic combustion of soot with a O_2/NO mixture. KNO_3/ZrO_2 catalysts, Catal. Commun. 4 (2003) 124–128.
[41] J. Liu, Z. Zhao, C.M. Xu, A.J. Duan, G.Y. Jiang, The structures, adsorption characteristics of La–Rb–Cu–O perovskite-like complex oxides, and their catalytic performances for the simultaneous removal of nitrogen oxides and diesel soot, J. Phys. Chem. C 112 (2008) 5930–5941.
[42] T. Seyama, Total oxidation of hydrocarbons on perovskite oxides, Catal. Rev. 34 (1992) 281–300.
[43] N. Yamazoe, Y. Teraoka, Oxidation catalysis of perovskites-relationships to bulk structure and composition (valency, defect, etc.), Catal. Today 8 (1990) 175–199.
[44] G. Saracco, F. Geobaldo, G. Baldi, Methane combustion on Mg-doped $LaMnO_3$ perovskite catalysts, Appl. Catal. B: Environ. 20 (1999) 277–288.
[45] L. Forni, I. Rossetti, Catalytic combustion of hydrocarbons over perovskites, Appl. Catal. B: Environ. 38 (2002) 29–37.
[46] N. Russo, D. Fino, G. Saracco, V. Specchia, Studies on the redox properties of chromite perovskite catalysts for soot combustion, J. Catal. 229 (2005) 459–469.
[47] D. Fino, N. Russo, E. Canda, G. Saracco, V. Specchia, La–Li–Cr perovskite catalysts for diesel particulate combustion, Catal. Today 114 (2006) 31–39.
[48] J. Oi-Uchisawa, A. Obuchi, R. Enomoto, J. Xu, T. Nanba, S. Liu, S. Kushiyama, Oxidation of carbon black over various Pt/MO_x/SiC catalysts, Appl. Catal. B: Environ. 32 (2001) 257–268.
[49] S. Liu, A. Obuchi, J. Oi-Uchisawa, T. Nanba, S. Kushiyama, An exploratory study of diesel soot oxidation with NO_2 and O_2 on supported metal oxide catalysts, Appl. Catal. B: Environ. 37 (2002) 309–319.
[50] K. Ito, K. Kishikawa, A. Watajima, K. Ikeue, M. Machida, Soot combustion activity of NOx-sorbing Cs–MnOx–CeO_2 catalysts, Catal. Commun. 8 (2007) 2176–2180.